

Chemical abundances and ionizing clusters of H II regions in the LINER galaxy NGC 4258

Angeles I. Díaz,¹★ Marcelo Castellanos,¹ Elena Terlevich²★† and María Luisa García-Vargas³

¹*Departamento de Física Teórica, C-XI, Universidad Autónoma de Madrid, 28049 Madrid, Spain*

²*INAOE, Tonantzintla, Apdo Postal 51, 72000 Puebla, México*

³*Grantecan S.A., 38200 La Laguna, Tenerife, Spain*

Accepted 2000 May 22. Received 2000 February 14; in original form 1999 September 8

ABSTRACT

We present long-slit observations in the optical and near-infrared of eight H II regions in the spiral galaxy NGC 4258. Six of the observed regions are located in the south-east inner spiral arms, and the other two are isolated in the northern outer arms. A detailed analysis of the physical conditions of the gas has been performed. For two of the regions, an electron temperature has been derived from the [S III] $\lambda 6312$ line. For the rest, an empirical calibration based on the red and near-infrared sulphur lines has been used. The oxygen abundances derived by both methods are found to be significantly lower (by a factor of 2) than previously derived by using empirical calibrations based on the optical oxygen lines.

In the brightest region, 74C, the observation of a prominent feature caused by Wolf–Rayet (WR) stars provides an excellent constraint over some properties of the ionizing clusters. In the light of the current evolutionary synthesis models, no consistent solution is found to explain at the same time both the WR feature characteristics and the emission-line spectrum of this region. In principle, the presence of WR stars could lead to large temperature fluctuations and also to a hardening of the ionizing radiation. None of these effects is found in region 74C, for which the electron temperatures found from the [S III] $\lambda 6312$ line and the Paschen discontinuity at 8200 Å are equal within the errors, and the effective temperature of the ionizing radiation is estimated at around 35 300 K.

Both more observations of confirmed high-metallicity regions and a finer metallicity grid for the evolutionary synthesis models are needed in order to understand the ionizing populations of H II regions.

Key words: stars: Wolf–Rayet – H II regions – galaxies: individual: NGC 4258 – galaxies: stellar content – galaxies: structure.

1 INTRODUCTION

Theoretically, the evolution of a young stellar population depends on metallicity at least through two very important effects: the increasing opacity of the stellar material, and the dependence of mass loss on metal content in high-mass stars. As a consequence of the first, the effective temperature of ionizing stars should be lower in regions of higher metallicity (see e.g. McGaugh 1991); on the other hand, as a consequence of the second, i.e. if the strength of stellar winds increases with metallicity, the loss of the outer envelopes of the most massive stars can increase their surface temperature to very high values. These highly evolved

massive O stars are identified with the Wolf–Rayet (WR) population.

Most theoretical evolutionary models for ionizing star clusters predict the appearance of WR stars – although at slightly different cluster ages depending on the specific details of the models – and in all of them the fraction of WR stars increases with metallicity, since the limiting mass for a star to enter the WR phase decreases with increasing metallicity. However, the effect of these stars on their surrounding ionized gas depends on the characteristics of the assumed wind opacity, and therefore, while some models predict the existence of high-metallicity H II regions of high excitation (e.g. García-Vargas & Díaz 1994; Stasińska & Leitherer 1996), others do not (e.g. Cerviño & Mas-Hesse 1994). The finding of this extreme H II region population would constitute firm evidence for the existence of WR stars with high effective temperatures,

★ E-mail: angeles@astro4.ft.uam.es (AID); et@ast.cam.ac.uk (ET)

† Visiting Fellow, Institute of Astronomy, Cambridge.

thus favouring the first kind of model; but, even if these regions are not definitively identified, the study of high-metallicity H II regions is of crucial importance to investigate the processes of star formation and evolution in high-metallicity environments.

This investigation gains even more relevance if we take into account recent observations that point to a firm connection between star formation and activity in active galactic nuclei (Heckman et al. 1997; González-Delgado et al. 1998) already predicted on theoretical grounds (Terlevich & Melnick 1985; Terlevich et al. 1992), since these nuclei seem to reach rather high metallicities (Phillips et al. 1984; González-Delgado & Pérez 1996), as deduced from the study of their circumnuclear star-forming regions.

Unfortunately, the term ‘high-metallicity H II region’ is rather ill-defined. Most authors apply the term to H II regions of solar or oversolar metal content, but the difficulty of deriving directly the metallicity of these cool H II regions is well known, and the empirical calibrations commonly employed provide estimations with an uncertainty larger than a factor of 2 (see e.g. Díaz et al. 1991). On the other hand, the characteristics of WR features are highly dependent on metallicity. Both the luminosity of the WR ‘bump’, i.e. the combination of the N III and He II lines at around $\lambda 4660$, and its equivalent width are predicted to be largest at the highest metallicity, and almost an order of magnitude difference is found between the computed WR ‘bump’ intensity relative to H β in clusters of half-solar and solar metallicities (Schaefer & Vacca 1998). Therefore, the detection of WR features combined with a detailed analysis of the emission-line spectra of suspected high-metallicity H II regions can constitute excellent tools for the simultaneous determination of both the metallicity and the age rather accurately in these regions.

In the frame of a long-term programme to study high-metallicity H II regions, we are presently carrying out a search for the high-metallicity and high-excitation H II region population by performing spectrophotometric observations at a resolution high enough to detect and measure WR features. For that, we have selected from the literature the giant H II regions with solar or oversolar abundance, as deduced from empirical calibrations based on the optical forbidden lines, showing the highest excitation. This corresponds to a ratio $[O III]/H\beta \sim 1.0$, which is actually quite moderate but still high compared to that expected in high-metallicity H II regions. Here we present the first of these investigations involving several H II regions in the galaxy NGC 4258.

NGC 4258 (M106) is classified as SAB(s)bc and Sb(s)II type by de Vaucouleurs, de Vaucouleurs & Corwin (1976) and Sandage & Tammann (1981) respectively. Heckman (1980) and Stauffer (1982) classified its nucleus as belonging to a transition type between a low-ionization nuclear emission region (LINER) galaxy and an H II region like emission-line galaxy. As addressed by Courtés et al. (1993, hereafter C93), the H II region distribution is very peculiar in the sense that three general structures are found: the normal spiral arms, with dense and very bright H II regions following pure spiral shapes as a consequence of the barred spiral type of this galaxy; the faint outer arms (H II region poor); and the anomalous spiral arms, discovered by Courtés & Cruveller (1961), without star formation and with no evidence of very blue stars (Deharveng & Pellet 1970). It is assumed that the anomalous arms were formed by powerful jets ejected by the active nucleus of the galaxy. Stüwe, Schulz & Hühnermann (1992) showed that the active nucleus must be obscured along the line of sight, as is also indicated by its invisibility in *IUE* spectra.

Cecil, Morse & Veilleux (1995) found, from the emission-line flux ratios, LINER-like gaseous excitation along the jets. They also point out the possibility that the circumnuclear region has undergone recent formation of massive stars induced by the jets that are flowing into the disc. However, no evidence for this star formation has been found, maybe as a result of the obscuration by molecular gas along the line of sight. Finally, a subparsec-diameter gaseous disc shows Keplerian motion around the centre of the galaxy, which indicates the presence of a mass of $3.6 \times 10^7 M_{\odot}$ within a radius of less than 0.13 pc (Miyoshi et al. 1995). This is probably the best existing evidence for the presence of a massive black hole at the centre of a galaxy.

The problem of the distance determination for this galaxy still remains unsolved. The quoted distance values range from 3.4 Mpc (Roy, Arsenault & Joncas 1986) to 10.4 Mpc (Sandage & Tammann 1981). The value adopted in the present work is 5.5 Mpc (Martin et al. 1989).

We have observed eight H II regions along two different spiral arms. Four of them have been identified as: 74C, 69C, 5N(A) and 5N(B) in C93. Regions 5N(A) and 5N(B) are located in the northern outer arm at a galactocentric distance of 20.3 kpc. The other six regions are located in the south-east inner arm at 8.05 kpc from the galaxy centre. Region 74C is a discrete radio source at 4.9 GHz (Hummel, Krause & Lesch 1989).

Regions 74C and 5N were previously observed by Oey & Kennicutt (1993), who derived values of $12 + \log(O/H)$ of 8.87 and 8.74 for each of them, respectively (the solar value is 8.92). With a ratio of $[O III]$ to $H\beta$ of 0.98 and 1.44, both regions fit our selection criteria.

2 OBSERVATIONS AND REDUCTIONS

Our spectrophotometric observations were obtained with the 4.2-m William Herschel Telescope (WHT) at the Roque de los Muchachos Observatory, on 1994 March 13, using the ISIS double spectrograph, with the TEK1 and EEV charge-coupled device (CCD) detectors in the blue and red arm, respectively. Two gratings were used, R300B in the blue and R316R in the red arm, covering from $[O II] \lambda 3727$ to $[S III] \lambda 9532$ in three different spectral ranges of $\sim 1700 \text{ \AA}$ each. The dispersion of $1.4 \text{ \AA pixel}^{-1}$ with a slit width of $1''.5$ gives a spectral resolution of $\sim 4 \text{ \AA}$. The nominal spatial sampling is $0''.7 \text{ pixel}^{-1}$. The seeing was $\sim 1''.5$. The slit was centred at the positions of regions 74C and 5N, as given by Oey & Kennicutt (1993). A third position was observed in order to include other H II regions outlining the south-east inner arm. In all cases the position angle was chosen to maximize the number of H II regions in the slit. A journal of observations is given in Table 1.

The data were reduced using the IRAF (Image Reduction and Analysis Facility) package following standard methods. The two-dimensional wavelength calibration was accurate to 1 \AA in all cases. The two-dimensional frames were flux-calibrated using two spectroscopic standard stars observed during the same night with a 5-arcsec slit width. The agreement between the individual calibration curves was better than 8 per cent in all cases. The spectra were previously corrected for atmospheric extinction using a mean extinction curve applicable to the La Palma observing site. The removal of the atmospheric water vapour absorption bands in the near-infrared (Díaz, Pagel & Wilson 1985) was achieved by dividing by the relatively featureless continuum of a subdwarf star observed during the same night as the galaxy.

Table 1. Journal of observations (all of which were made on 1994 March 13/14).

PA (°)	Grating	λ range (Å)	Exposure (s)
255	R300B	3675–5300	1800
255	R300B	3675–5300	1800
255	R316R	5890–7600	1200
255	R316R	5890–7600	1800
255	R316R	7960–9670	1800
255	R316R	7960–9670	1800
150	R300B	3675–5300	1800
150	R300B	3675–5300	1800
150	R300B	3675–5300	1200
150	R316R	5890–7600	1800
150	R316R	7960–9670	1800
150	R316R	7960–9670	1800
133	R300B	3675–5300	1800
133	R300B	3675–5300	1200
133	R316R	5890–7600	1800
133	R316R	7960–9670	1800

The most critical step in the reduction process was the background subtraction in the near-infrared frames. There are numerous OH emission lines of the night-sky spectrum that contaminate the near-infrared spectra. This contamination is particularly important in the range from 9376 to 9600 Å (Osterbrock, Fulbright & Bida 1997). Hence, the intensities of the [S III] λ 9532 and Pa 8 lines could be affected even after the background subtraction is carried out. Fortunately, the [S III] λ 9069 and Pa 9 lines are unaffected by these night-sky lines. The observed λ 9532/ λ 9069 ratio is above the theoretical value of 2.44 in four of the observed regions. In these cases, the [S III] λ 9532 line was scaled by means of the more accurate [S III] λ 9069 line intensity measurement.

3 RESULTS

Fig. 1 shows the spatial distribution of the H α flux along the slit for the three different positions observed. Regions 5N(A) and 5N(B) are clearly identified on the H α profile corresponding to position angle PA = 255°. Also regions 74C and 69C, showing a certain degree of substructure, are resolved at PA = 133°. Four different regions are resolved at PA = 150°, which we have named GA1, GA2, GA3 and GA4. A fifth region is clearly seen in the H α profile that is not detected in the near-IR frames.

The spectra corresponding to each of the identified regions are shown in Figs 2–6. WR features around λ 4680 are seen in the spectrum of region 74C and to a lesser extent in that of region 5N.

3.1 Line intensities

Emission-line fluxes were measured using the IRAF SPLIT software package, by integrating the line intensity over a local fitted continuum. The errors in the line fluxes have been calculated from the expression

$$\sigma_l = \sigma_c N^{1/2} [1 + \text{EW}/(N\Delta)]^{1/2},$$

where σ_l is the error in the line flux, σ_c represents the standard deviation in a box near the measured emission line and stands for the error in the continuum placement, N is the number of pixels used in the measurement of the line flux, EW is the line equivalent width, and Δ is the wavelength dispersion (Å pixel⁻¹).

The observed line intensities relative to the H β line were corrected for interstellar reddening according to an average

extinction curve (Osterbrock 1989) and assuming the Balmer line theoretical values for case B recombination (Brocklehurst 1971). The presence of an underlying stellar population is evident in the blue spectra of regions GA2, GA3 and GA4. The H γ and H δ Balmer lines are clearly affected by this stellar absorption. An iterative process was applied in order to fit observed and theoretical Balmer line intensities and to obtain the reddening constant $c(\text{H}\beta)$. In all cases, H α , H γ and H δ were fitted, except in regions GA3 and GA4, for which H δ seems to be underestimated. Reddening-corrected Paschen lines, when measured, are consistent with their theoretical values.

The reddening-corrected line intensities together with their corresponding errors are given in Table 2 for regions 74C and 69C and in Table 3 for the rest of the regions. Also given in the tables are the extinction-corrected H α flux and the H β equivalent width. For all the regions, H α luminosities are lower than 10³⁸ erg s⁻¹, with the exception of region 74C, in which a value of 10^{39.3} erg s⁻¹ is found. According to Kennicutt (1983), this region can be classified as a supergiant H II region.

3.2 Physical conditions of the gas

Electron densities for each observed region were derived from the ratio of the [S II] λ 6717/ λ 6731 lines following standard methods (see e.g. Osterbrock 1989). For regions GA2 and 74C densities of 160 and 60 cm⁻³ respectively are obtained. For the rest of the regions the ratio of the [S II] lines implies $n_e \leq 40$ cm⁻³.

For two of the observed regions, 74C and 69C, it has been possible to measure the weak auroral [S III] λ 6312 line, which, together with the observed intensities of the nebular lines at λ 9069, 9532, can be used to obtain a value for the electron temperature. Using the expressions given by Osterbrock (1989) and the effective collision strengths recently calculated by Tayal (1997), we find for $t(\text{S}^{2+})$ values of 7500 ± 300 K and 7600 ± 500 K for regions 74C and 69C, respectively.

Photoionization models indicate that, for abundances close to solar, the region where sulphur is twice ionized overlaps the regions of both once and twice ionized oxygen, and therefore $t(\text{S}^{2+})$ is expected to be intermediate between $t(\text{O}^+)$ and $t(\text{O}^{2+})$. Garnett (1992), from single-star photoionization models, finds a linear relation between the temperatures of O²⁺ and S²⁺:

$$t(\text{O}^{2+}) = 1.20 t(\text{S}^{2+}) - 0.20. \quad (1)$$

We have used that relation to obtain $t(\text{O}^{2+})$. Finally, Stasińska's (1980) relation between $t(\text{O}^{2+})$ and $t(\text{O}^+)$ has been used to calculate the temperature of the $t(\text{O}^+)$ zone. These different temperatures for regions 74C and 69C are listed in Table 4.

Another independent way of temperature determination is through the measure of the Paschen discontinuity at λ 8200. The ratio of the Paschen discontinuity to the H β intensity is, after correcting for the derived extinction value of $c(\text{H}\beta) = 0.48$, given by

$$\frac{\Delta\text{Pa}}{I(\text{H}\beta)} = (6.9 \pm 0.8) \times 10^{-15} \text{ Hz}^{-1}. \quad (2)$$

According to the models computed by González-Delgado et al. (1994), for the helium abundance derived for the region 74C (see next section), this $\Delta\text{Pa}/I(\text{H}\beta)$ implies an electron temperature of 8000 ± 700 K, which agrees with that derived from the [S III] lines within the errors. Therefore, no temperature fluctuations are

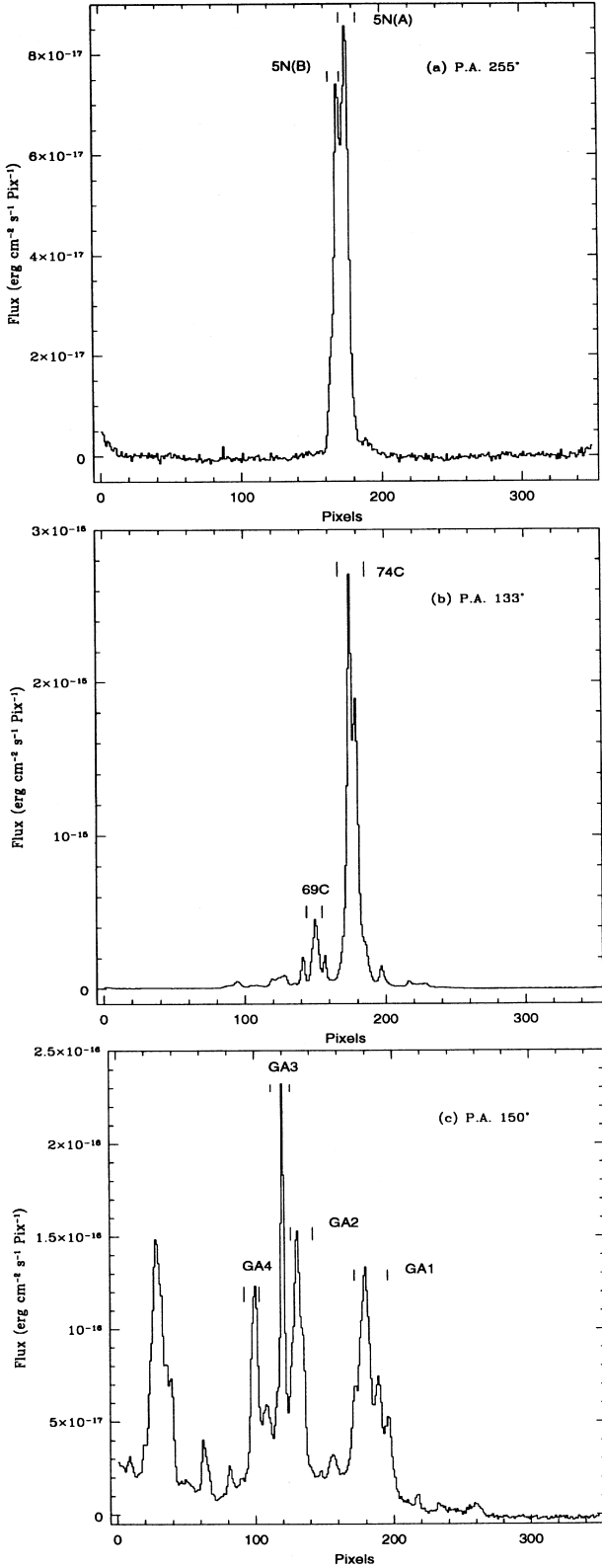


Figure 1. $H\alpha$ profiles for the three observed slit positions including: (a) regions 5N(A) and 5N(B); (b) regions 74C and 69C; and (c) regions GA1, GA2, GA3 and GA4.

apparent in the region which might have been expected from the presence of WR stars (Pérez 1997).

For the rest of the regions it was not possible to obtain a direct measure of the electron temperature. An average temperature has been adopted from an empirical calibration by means of the sulphur abundance parameter (Díaz & Pérez-Montero 2000)

$$S_{23} = ([S\text{ II}]\lambda 6717, 6731 + [S\text{ III}]\lambda 9069, 9532)/H\beta.$$

The values for these temperatures, together with similar ones derived for regions 74C and 69C, are also given in Table 4.

3.3 Chemical abundances

Ionic abundances of oxygen, nitrogen and sulphur have been derived following standard methods (Pagel et al. 1992) and using the temperatures found above. These abundances are listed in Table 4. We have assumed that most of the oxygen and sulphur are in the first and second ionization stages, and therefore

$$O/H = O^+/H^+ + O^{2+}/H^+$$

and

$$S/H = S^+/H^+ + S^{2+}/H^+.$$

This assumption seems to be justified given the relatively low estimates of the electron temperature.

The helium abundance was determined from the $\text{He I } \lambda\lambda 4471, 6678$ lines. Mean values of 0.070 ± 0.005 and 0.060 ± 0.005 , respectively, are obtained for regions 74C and 69C. We have estimated the contribution of neutral helium from the expression (Kunth & Sargent 1983):

$$\text{He}^0 + \frac{\text{He}^+}{H^+} = \left(1 - 0.25 \frac{O^+}{O}\right)^{-1} \frac{\text{He}^+}{H^+}. \quad (3)$$

The correction factors obtained for regions 74C and 69C are 1.17 and 1.20, respectively, which yield He abundances $y = 0.081$ for region 74C and $y = 0.068$ for region 69C.

3.4 Wolf-Rayet features

A prominent Wolf-Rayet feature has been observed in region 74C (see Fig. 7). Assuming a distance to NGC 4258 of 5.5 Mpc (Martin et al. 1989) and a constant extinction value through this region of $c(H\beta) = 0.48$, as derived from the Balmer and Paschen recombination lines, the total luminosity of the broad He II feature, without the contribution of the $[\text{Fe III}] \lambda 4658$ line, is $(1.1 \pm 0.1) \times 10^{38} \text{ erg s}^{-1}$. This value comprises the broad features of both $\text{N III } \lambda\lambda 4634, 4640$ and $\text{He II } \lambda 4686$ lines. The contribution of the N III lines to the WR bump is metallicity-dependent according to Smith (1991). In our case this contribution represents 0.4 times the total emission; hence we obtain for the He II line luminosity:

$$L(\text{He II } \lambda 4686) = (6.6 \pm 0.6) \times 10^{37} \text{ erg s}^{-1}. \quad (4)$$

The non-detection of $\text{N V } \lambda\lambda 4604, 4620$ suggests that the WR stars are of late N or intermediate type. Using the calibration of Vacca & Conti (1992), 38 ± 5 WN stars are found in this region.

Another fainter Wolf-Rayet feature has been observed in region 5N(A). The bump luminosity is $2.2 \times 10^{36} \text{ erg s}^{-1}$. The contribution of the N III lines represents 0.45 times the total emission, hence the He II line luminosity is $1.2 \times 10^{36} \text{ erg s}^{-1}$, which is compatible with the presence of one WN star.

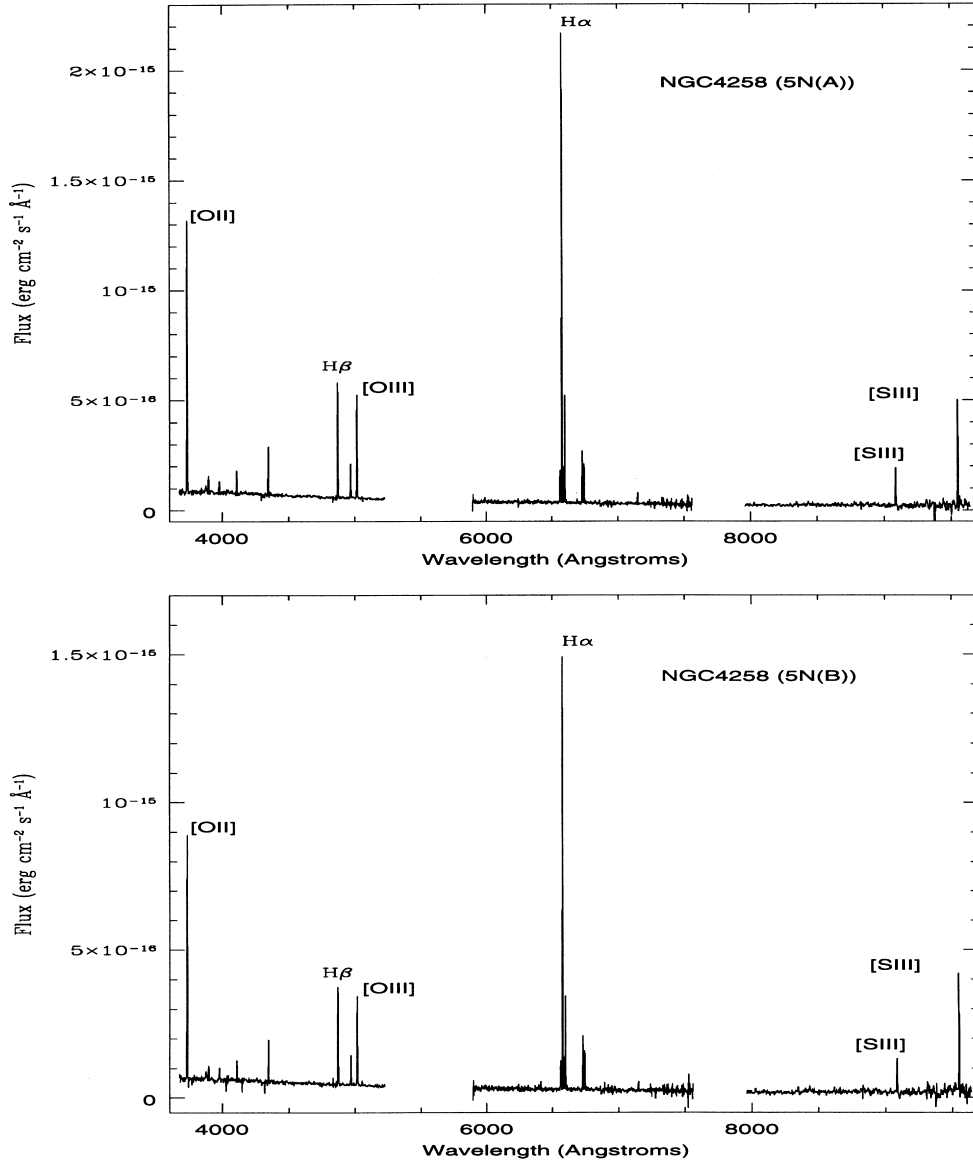


Figure 2. Merged spectra for the regions 5N(A) and 5N(B).

4 FUNCTIONAL PARAMETERS OF THE OBSERVED H II REGIONS

There are three fundamental parameters that control the emission-line spectra of H II regions (Díaz et al. 1991): the ionization parameter, the shape of the ionizing continuum, and the metallicity.

The ionization parameter – i.e. the ratio of the ionizing photon density to the particle density – is a measure of the degree of ionization of the nebula, and can be deduced from the ratio of two lines of the same element corresponding to two different ionization states, e.g. [O II]/[O III] or [S II]/[S III]. Alternatively, it can also be determined from [O II]/Hβ or [S II]/Hα if the metallicity of the region is known (Díaz 1994). By using a large grid of single-star photoionization models, the following expressions are found (Díaz et al. 1991; Díaz 1999):

$$\log U = -1.39 \log([O II]/H\beta) + 0.87 \log(Z/Z_{\odot}) - 1.68, \quad (5)$$

$$\log U = -1.40 \log([S II]/H\beta) + 1.10 \log(Z/Z_{\odot}) - 3.26, \quad (6)$$

$$\log U = -0.80 \log([O II]/[O III]) - 3.02, \quad (7)$$

$$\log U = -1.68 \log([S II]/[S III]) - 2.99. \quad (8)$$

We have derived U from the four expressions above. In all cases the value of U derived from the [O II]/[O III] ratio is systematically lower than the rest, thus implying low effective temperatures for the ionizing stars (see e.g. Díaz 1999). We have therefore discarded this value and computed U as the mean of the other three. These adopted ionization parameters – $\log U$ – are listed in Table 5 and their uncertainty is estimated to be around ± 0.2 dex.

The shape of the ionizing continuum is directly related to the effective temperature of the stars that dominate the radiation field responsible for the ionization of the nebula. A recent version of the photoionization code CLOUDY (Ferland 1996) has been used to estimate the mean effective temperature of these stars. We have used Mihalas' non-local thermodynamic equilibrium (NLTE) single-star stellar atmosphere models, with a closed geometry

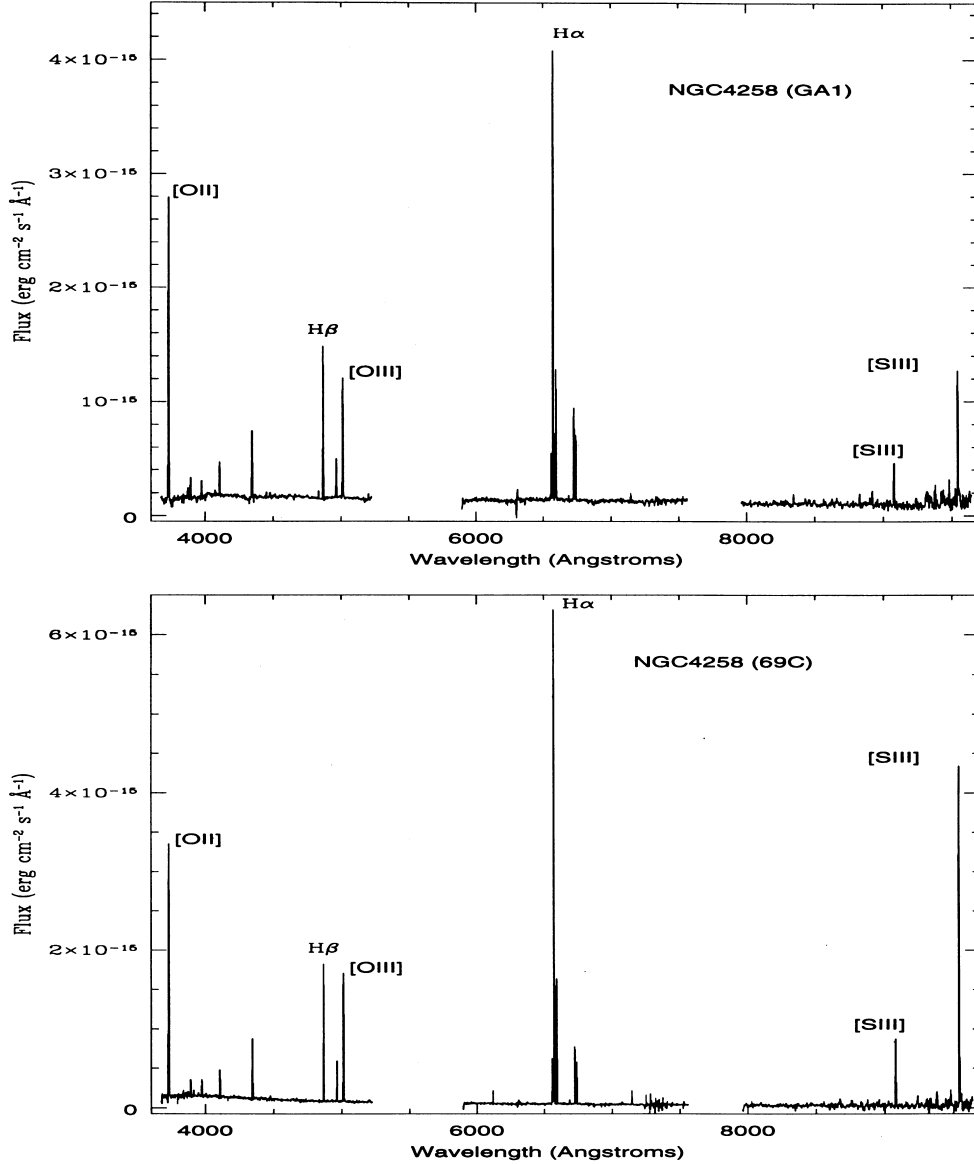


Figure 3. Merged spectra for the regions GA1 and 69C. They could correspond to different regions of the same nebula.

and a constant particle density through the nebula. For all the regions, consistency is found for effective temperatures around 35 000–36 000 K. The results from these photoionization models compared to the observations are presented in Table 5.

5 DISCUSSION

The $H\alpha$ fluxes for regions 74C and 69C, uncorrected for reddening, are 2692 and $287 \times 10^{-16} \text{ erg s}^{-1} \text{ cm}^{-2}$, respectively. These fluxes are to be compared with 3492 and $332 \times 10^{-16} \text{ erg s}^{-1} \text{ cm}^{-2}$ measured by C93. Considering that our observations have been obtained through a narrow slit and region 74C is rather extended, the agreement can be considered satisfactory. The combined $H\alpha$ flux of our regions 5N(A) and 5N(B) is $187 \times 10^{-16} \text{ erg s}^{-1} \text{ cm}^{-2}$, close to the value of $249 \times 10^{-16} \text{ erg s}^{-1} \text{ cm}^{-2}$ given by C93 for region 5N. Regarding the rest of the regions, we tentatively identify regions GA2, GA3 and GA4 with regions 59C, 58C and 54C of C93. Region GA1 probably corresponds to the outer parts of region 69C.

For each of our observed regions we have calculated the $H\alpha$ luminosity and the number of hydrogen ionizing photons from the observed $H\alpha$ flux corrected for their derived reddening (see Tables 2 and 3). Both quantities depend on the distance D to NGC 4258 according to the expressions:

$$L(H\alpha) = 3.62 \times 10^{37} \left[\frac{F(H\alpha)}{10^{-14}} \right] \left(\frac{D}{5.5} \right)^2 \text{ erg s}^{-1}, \quad (9)$$

$$Q(H) = 2.65 \times 10^{49} \left[\frac{F(H\alpha)}{10^{-14}} \right] \left(\frac{D}{5.5} \right)^2 \text{ photon s}^{-1}, \quad (10)$$

where $F(H\alpha)$ is expressed in $\text{erg s}^{-1} \text{ cm}^{-2}$ and D is given in Mpc.

These values are given in Table 6 for the adopted distance of 5.5 kpc. Only region 74C has an $H\alpha$ luminosity greater than $10^{39} \text{ erg s}^{-1}$ and can be classified as a supergiant H II region as defined by Kennicutt (1983). The rest of the regions have $H\alpha$ luminosities typical of H II regions in early spiral galaxies, although all of them are greater than $10^{37} \text{ erg s}^{-1}$ [$Q(H) >$

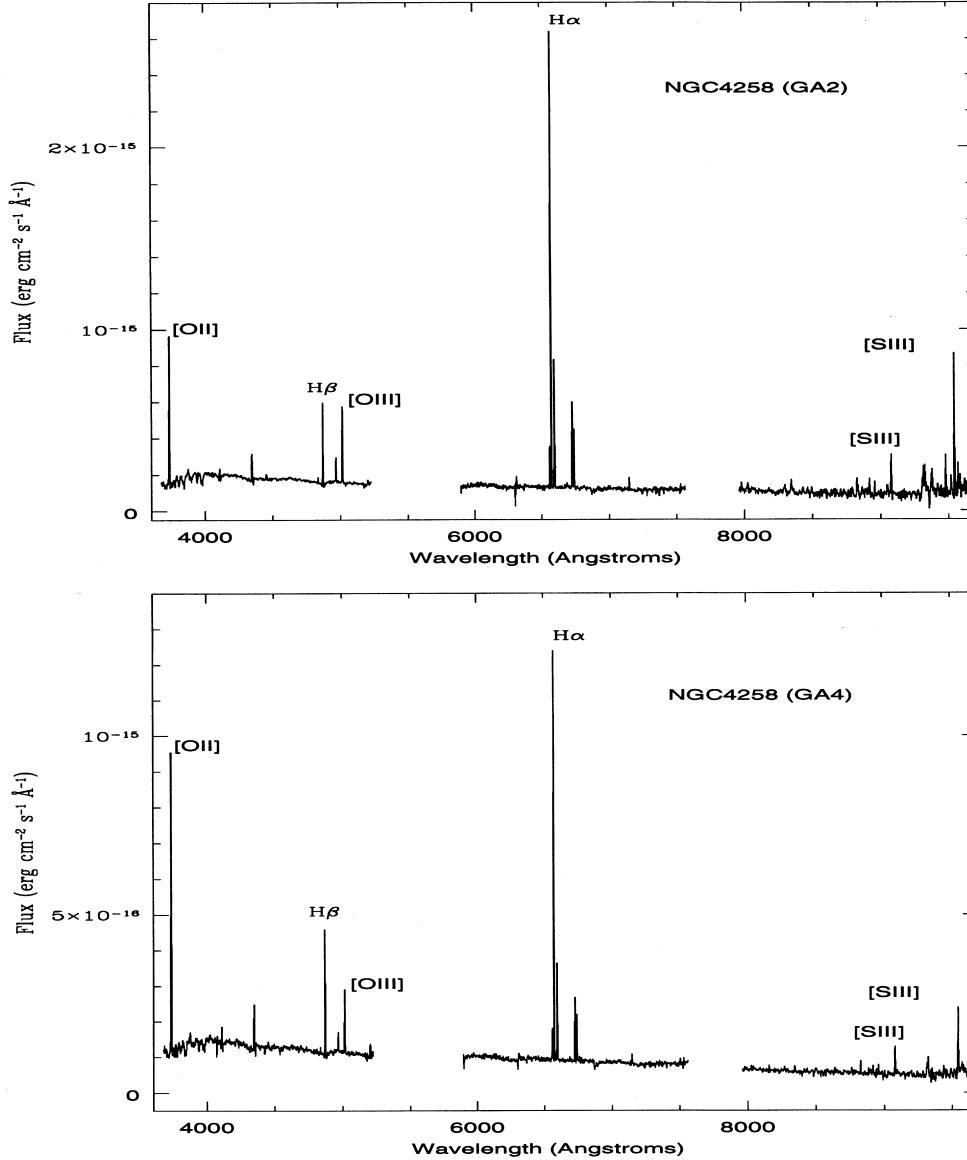


Figure 4. Merged spectra for the regions GA2 and GA4.

10^{49} photons s^{-1}], requiring more than a single star for their ionization (Panagia 1973).

Filling factors for each observed region can be determined from the reddening-corrected $H\alpha$ flux, $F(H\alpha)$, and the derived ionization parameter, U , according to the expression:

$$\epsilon = 0.34 \left[\frac{F(H\alpha)}{10^{-14}} \right]^{-1/2} \left(\frac{D}{5.5} \right)^{-1} \left(\frac{U}{10^{-3}} \right)^{3/2} \times \left[\frac{\alpha_B(H^0, T)}{10^{-13}} \right]^{-1} \times \left(\frac{n_e}{100} \right)^{-1/2}, \quad (11)$$

where $\alpha_B(H^0, T)$ is the recombination coefficient for hydrogen and n_e is the electron density of the emitting gas. The filling factors computed in this way are listed in Table 6. We have used a value of $\alpha_B(H^0, T) = 3.76 \times 10^{-13} \text{ cm}^3 \text{ s}^{-1}$, corresponding to $T = 7000 \text{ K}$ and $n_e = 100 \text{ cm}^{-3}$ (Osterbrock 1989). For regions 74C and GA2 we have used values of $n_e = 60$ and 160 cm^{-3} , respectively, as derived from the ratio between the red [SII] lines. For the rest of the regions for which only upper limits to the

density could be derived, a value of $n_e = 10 \text{ cm}^{-3}$ has been assumed.

According to C93 the angular sizes of regions 74C, 69C and 5N are 38.6, 16.8 and 20.5 arcsec, respectively. The corresponding linear sizes, at the assumed distance to NGC 4258, are 1.0, 0.45 and 0.55 kpc. These are comparable to the sizes of HII regions of moderate intensity found in other spiral galaxies (e.g. González-Delgado et al. 1997).

$H\alpha$ angular effective diameters – i.e. the diameters containing half the $H\alpha$ emission – of regions 74C, 69C and 5N are 4.3, 3.7 and 6.1 arcsec, respectively (C93), which translate into 115, 99 and 163 pc. From the definition of U it is possible to obtain the angular size of the emitting region using the reddening-corrected $H\alpha$ flux and the derived electron density:

$$\left(\frac{\phi}{10''} \right) = 0.06 \left[\frac{F(H\alpha)}{10^{-14}} \right]^{1/2} \left(\frac{U}{10^{-3}} \right)^{-1/2} \left(\frac{n_e}{100} \right)^{-1/2}, \quad (12)$$

where ϕ is the angular diameter in units of 10 arcsec. This angular diameter does not depend on the assumed distance to the galaxy.

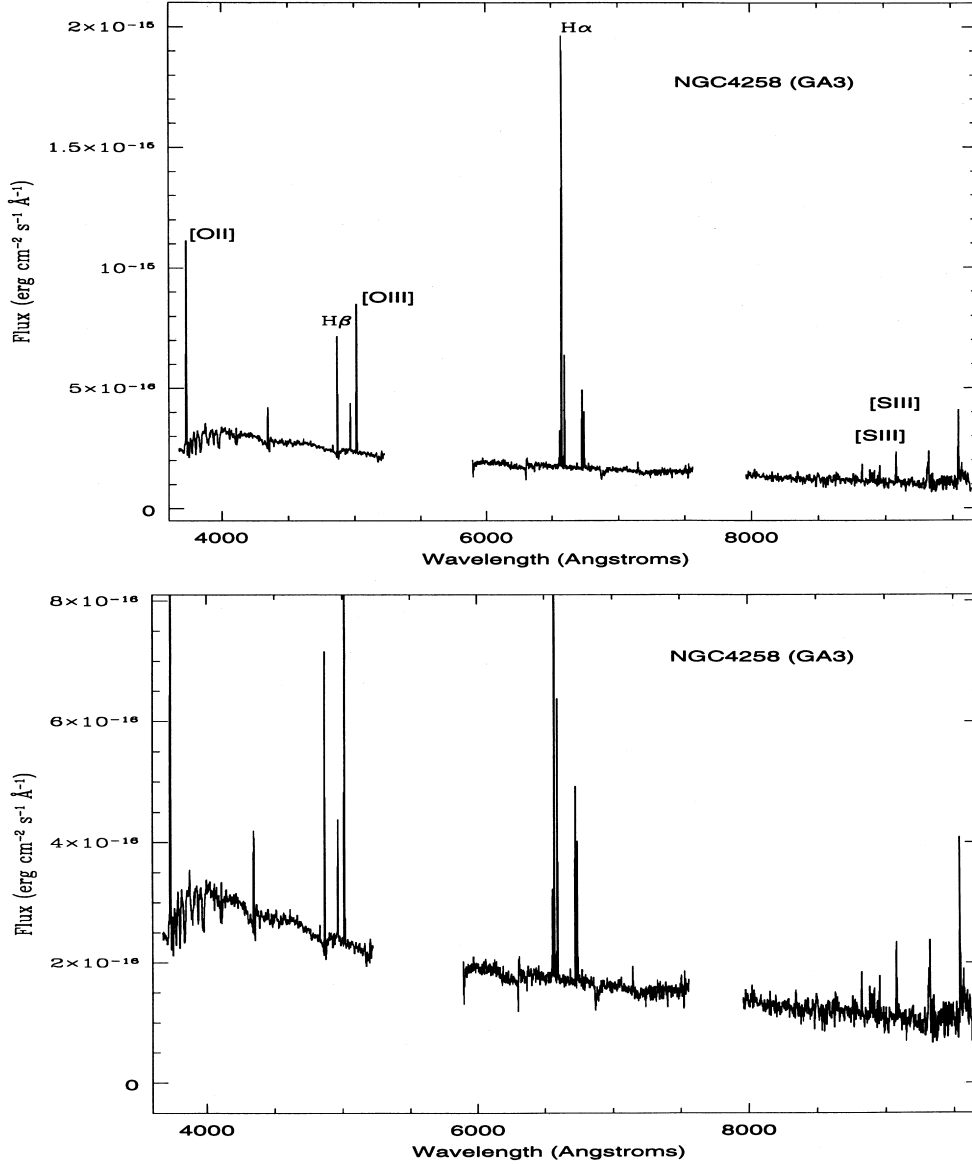


Figure 5. Merged spectra for region GA3. The bottom panel is an enlargement to show the prominent absorption features.

For region 74C the derived angular diameter is 3.3 arcsec, close to the value of 4.3 arcsec given by C93. For region 69C their observed value of the effective diameter of 3.7 arcsec yields a value of the electron density of $n_e = 5 \text{ cm}^{-3}$, close to the assumed one of 10 cm^{-3} . Using this value of n_e for the rest of the observed regions, except GA2 for which $n_e = 160 \text{ cm}^{-3}$, we obtain angular diameters between 1 and 2.6 arcsec.

We can also calculate the mass of ionized hydrogen following the expression (Osterbrock 1989):

$$M(\text{H II}) = \frac{m_p Q(\text{H})}{n_e (1 + y^+) \alpha_B (H^0, T)}, \quad (13)$$

where m_p is the mass of the proton and y is the abundance by number of ionized helium, which we have taken as 0.10. Using observed and derived quantities, this expression becomes

$$M(\text{H II}) = 538 \left[\frac{F(\text{H}\alpha)}{10^{-14}} \right] \left(\frac{n_e}{100} \right)^{-1} \left(\frac{D}{5.5} \right)^2 M_\odot. \quad (14)$$

The corresponding masses of ionized hydrogen in each observed region are given in Table 6.

From evolutionary models of single ionizing clusters and radiation-bounded H II regions, a relation between the number of ionizing $\text{Ly}\alpha$ photons per second per solar mass and the $\text{H}\beta$ equivalent width (Díaz 1999) can be found, which allows the estimation of the ionizing cluster mass by taking into account the cluster evolution:

$$\log[Q(\text{H})/M_\odot] = 0.86 \log[\text{EW}(\text{H}\beta)] + 44.48. \quad (15)$$

For our observed regions, all values for $Q(\text{H})$ are around $10^{49} \text{ photons s}^{-1}$, except for region 74C for which a value of the order of $10^{51} \text{ photons s}^{-1}$ is found. Hence, in the absence of dust, a lower limit for the mass of the ionizing clusters can be estimated by means of the $\text{H}\beta$ measured equivalent width and the $\text{H}\alpha$ luminosity for each region. The estimated ionizing cluster masses range from $4 \times 10^3 M_\odot$ for region GA4 to $1.12 \times 10^5 M_\odot$ for region 74C.

The high signal-to-noise ratio spectrum of this latter region

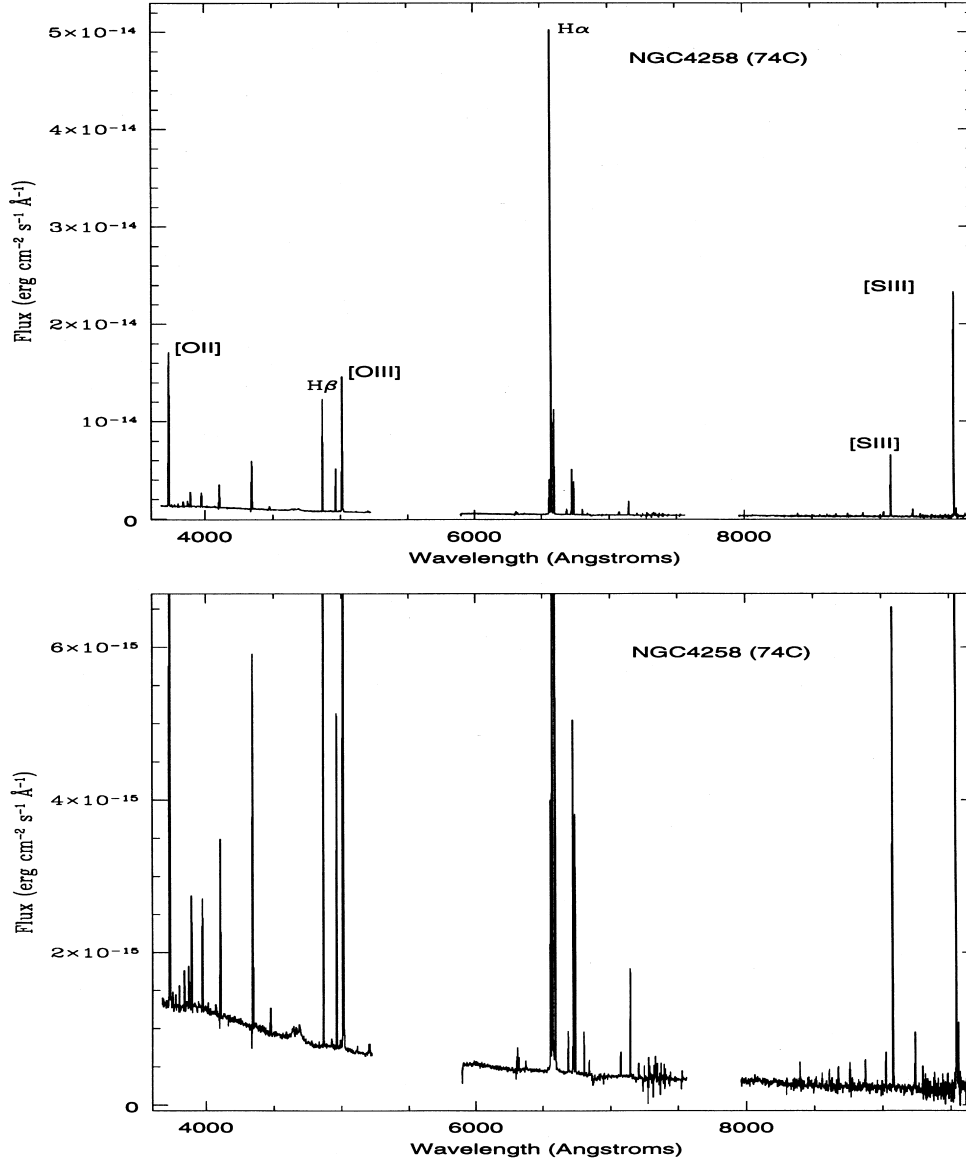


Figure 6. Merged spectra with two intensity scales for region 74C. Notice the WR feature at 4686 Å.

allows a more detailed modelling. The presence of WR features, in principle, provides a means to constrain the age of the ionizing population. The observed WR ‘bump’ luminosity relative to $H\beta$ [$L(\text{WR})/H\beta$] is 0.15. According to the models by Schaerer & Vacca (1998), at metallicity $Z = 0.008$ (0.4 solar), these high values are only found at an age of 4.5 Myr. However, this ratio is strongly dependent on metallicity, and changes by more than an order of magnitude between $Z = 0.008$ (0.4 solar) and $Z = 0.02$ (solar). Therefore, the slightly higher metallicity of region 74C ($Z \approx 0.012$) might allow earlier ages for the WR stellar population. Clearly, the available grid for stellar evolution models is too coarse to elucidate this matter. The same applies to the equivalent width of the ‘bump’ [EW(WR)], whose observed value is 10.8 Å. Since the N III $\lambda 4640$ line is strongly dependent on metallicity (Smith, Shara & Moffat 1996), it is probably more advisable to use only the flux and equivalent width of the He II line. In that case, our observed values of $L(\text{He II})/H\beta$ and EW(He II) are 0.09 and 6.6 Å respectively. Again, consistency is found for a model of $Z = 0.008$ and an age of 4.5 Myr.

Since, according to the recent evolutionary models of Leitherer et al. (1999, STARBURST99), the observed value of the equivalent width of $H\beta$ (81 Å) points also to an age of around 4.5 Myr, we have computed the emission-line spectrum corresponding to this single ionizing cluster. [All the models are computed assuming a standard Salpeter initial mass function for the stellar ionizing cluster and using the photoionization code CLOUDY (Ferland 1996).] This set of models makes use of the same evolutionary tracks as the models of Schaerer & Vacca (1998) and therefore provides a self-consistent frame. The results of the computation can be seen in Table 7 together with the observed emission-line ratios. It can be seen that the model ionizing spectrum is too hard and does not reproduce the observations. This is not surprising in view of the low effective temperature found from single-star photoionization models (Table 5). It can be better appreciated in Fig. 8, where the spectral energy distribution of the cluster can be compared to that of the Mihalas stellar atmosphere of a star with $T_{\text{eff}} = 35\,300$ K, which adequately reproduces the data. A high-energy tail is clearly

Table 2. Reddening-corrected line intensities for PA = 133°.

Line		Region	
		74C	69C
3727	[O II]	2100±40	2280±90
3751	H12	18±1	–
3770	H11	18±1	–
3798	H10	24±1	–
3835	H9 + He II	44±2	26±2
3868	[Ne III]	53±2	–
3888	H8 + He I	161±3	118±7
3902	[Ne III] + He I	151±4	122±6
4102	Hδ	251±5	220±10
4340	Hγ	468±7	450±20
4471	He I	33±2	30±2
4861	Hβ	1000±8	1000±20
4922	He I	7±1	–
4959	[O III]	378±5	290±10
4987	[Fe III]	7±1	–
5007	[O III]	1140±10	930±30
5012	He I	17±2	–
5200	[N I]	8±1	13±1
6300	[O I]	17±1	20±1
6312	[S III]	9±1	7±1
6360	[O I]	4±1	10±2
6548	[N II]	200±10	260±10
6563	Hα	2860±60	2850±40
6584	[N II]	610±20	780±20
6678	He I	30±2	22±2
6717	[S II]	260±10	363±8
6731	[S II]	188±3	253±7
7135	[Ar III]	74±2	66±4
8502	P16	4±1	–
8545	P15	6±1	–
8598	P14	6±1	–
8665	P13	10±1	–
8750	P12	11±1	–
8863	P11	15±1	–
9014	P10	19±1	–
9069	[S III]	266±4	190±10
9229	P9	27±2	26±3
9532	[S III]	660±20	930 ^a ±30
9546	P8	35±1	34±2
[6pt] $c(H\beta)$		0.48	0.08
$F(H\alpha)^b$		5576	321
EW(Hβ) (Å)		81	113

^aAffected by a cosmic ray.^b 10^{-16} erg cm⁻² s⁻¹, corrected for reddening.

present in the ionizing cluster as the result of the WR star contribution.

These models assume an enhanced mass loss during the evolution of massive stars, as prescribed by the stellar evolution models of Meynet et al. (1994). More moderate mass-loss rates are assumed in the models of Bressan et al. (1993) and Fagotto et al. (1994), and with them a single population of 5.3 Myr can adequately reproduce the emission-line spectrum (see Table 7). The corresponding ionizing spectrum is also shown in Fig. 8. However, this ionizing cluster provides only a few WR stars [about 3×10^{-5} per solar mass of the ionizing cluster, for a metallicity $Z = 0.008$ (García-Vargas, Bressan & Díaz 1995)]. This is probably not enough to reproduce the observed values of $L(WR)/H\beta$.

The WR features observed in region 74C are similar to those found in other extragalactic H II regions. Table 8 shows the values of the WR feature intensities and equivalent widths for 74C and three other well-studied extragalactic H II regions: NGC 604 in M33 (Díaz et al. 1987; Terlevich et al. 1996), region A in NGC

3310 (Pastoriza et al. 1993), and region A in NGC 7714 (García-Vargas et al. 1997). Also given in the table are the metallicities of the regions in the form $12 + \log(O/H)$ and the effective temperature of the ionizing radiation estimated from single-star photoionization models.

The tabulated values are difficult to explain in the light of the recent models of Schaerer & Vacca (1998). The expected decrease of the intensities of WR features with decreasing metallicity is not clearly observed. However, a decrease of the temperature of the ionizing radiation with increasing metallicity is apparent. In fact, region A in NGC 3310 and region 74C in NGC 4258 show the same $L(WR)/H\beta$ ratio despite their different metallicity (by a factor of about 3). This implies that both regions have similar ratio of WR to O stars, while, at the same time, their effective temperatures are considerably different.

The interpretation of the equivalent widths of WR features is even more difficult, since they may be affected by the continuum from any underlying stellar population. Composite populations have been postulated for region A in NGC 3310 (Pastoriza et al. 1993) and region A in NGC 7714 (García-Vargas et al. 1997). Under this assumption, the equivalent widths, EW(WR) and EW(He II), of the cluster with WR stars are increased to 6 and 4.8 Å for region A in NGC 3310 and to 3.6 and 2.5 Å for region A in NGC 7714, which might still be compatible with the Schaerer & Vacca models. In the case of region 74C, combinations of two ionizing clusters can be found that adequately reproduce the emission-line spectrum; however, this assumption would produce equivalent widths for the WR cluster higher than the maximum predicted for the models with $Z = 0.008$, although probably compatible with solar metallicity models. Again, a finer metallicity grid for the WR cluster synthesis models would be needed in order to explore this possibility in further detail.

6 SUMMARY AND CONCLUSIONS

We have analysed eight H II regions in the LINER galaxy NGC 4258 using spectrophotometric observations between 3700 and 9650 Å. For two of the regions it has been possible to measure the electron temperature from the [S III] λ6312 line, which allows the derivation of accurate abundances following standard methods. For the rest of the regions an empirical calibration based on the sulphur emission lines has been used to determine a mean oxygen content. The derived metallicities range from 0.3 to 0.6 Z_{\odot} . In particular, the metallicities found for regions 74C and 5N, previously reported by Oey & Kennicutt (1993) to be close to solar, are found to be lower by a factor of 2.

For each observed region, we have also estimated the functional parameters: the ionization parameter and the effective temperature of the ionizing cluster. Most regions show ionization parameters of the order of 10^{-3} and effective temperatures of around 35 300 K, except regions 74C and 69C for which higher ionization parameters are found. We have also derived the physical properties of the regions and their corresponding ionizing clusters: filling factor, mass of ionized gas, and mass of ionizing stars. Most of the regions, except 74C, have small ionizing clusters with masses in the range 4000 to 25 000 solar masses. These values constitute in fact lower limits, since the regions are assumed to be ionization-bounded and the presence of dust has not been taken into account.

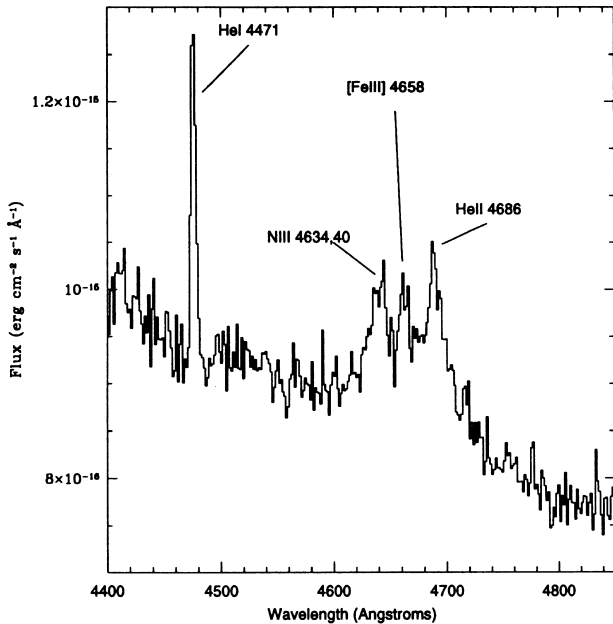
WR features have been detected in region 74C and, to a lesser extent, in region 5N(A). Detailed modelling has been carried out

Table 3. Reddening-corrected line fluxes for PA = 255° and 150°.

Line		5N(A)	5N(B)	Region			
				GA1	GA2	GA3	GA4
3727	[O II]	3300±100	3400±200	2340±80	3010±90	2100±100	2800±200
3770	H11	—	—	37±2	—	—	—
3798	H10	—	—	31±3	—	—	—
3888	H8 + He I	145±8	160±10	133±7	—	—	—
3902	[Ne III] + He II	125±6	136±9	105±7	—	—	—
4102	Hδ	240±10	250±20	240±10	220±10	150±20	190±30
4340	Hγ	450±20	480±30	450±10	400±10	390±30	380±20
4861	Hβ	1000±30	1000±40	1000±20	1000±20	1000±40	1000±30
4959	[O III]	290±10	280±20	270±10	260±10	390±20	160±10
5007	[O III]	840±30	840±40	790±20	860±20	1140±60	520±30
5200	[N I]	—	—	—	56±2	38±6	—
6548	[N II]	190±10	200±10	250±10	260±10	240±20	240±10
6563	Hα	2820±90	2880±90	2800±50	2800±30	2800±90	2850±90
6584	[N II]	640±20	630±30	780±20	790±10	760±30	700±20
6678	He I	28±2	—	22±2	21±2	17±3	15±2
6717	[S II]	310±20	350±20	560±10	500±10	520±30	450±20
6731	[S II]	220±10	240±20	440±10	360±10	370±20	320±10
7135	[Ar III]	64±5	59±4	42±8	64±3	51±5	67±5
9069	[S III]	210±20	200±20	300±20	180±10	210±20	230±20
9229	P9	26±3	27±3	25±3	—	—	27±3
9532	[S III]	590±40	500±60	750±50	450±50	470±40	540±50
$c(H\beta)$		0.35	0.39	0:	0.7	0.18	0:
$F(H\alpha)^a$		189	140	220	395	93	60
$EW(H\beta)$ (Å)		52	46	55	21	14	20

^a10⁻¹⁶ erg cm⁻² s⁻¹, corrected for reddening.**Table 4.** Derived physical conditions of the gas in the observed H II regions.

Parameter	74C	69C	5N(A)	5N(B)	GA1	GA2	GA3	GA4
n_e	60	≤40	≤40	≤40	≤40	160	≤40	≤40
$t(S^{2+})$	0.75±0.03	0.76±0.05	—	—	—	—	—	—
$t(O^{2+})$	0.69±0.04	0.72±0.05	—	—	—	—	—	—
$t(O^+)$	0.79±0.03	0.80±0.04	—	—	—	—	—	—
$\langle t \rangle_{\text{adop}}$	0.79	0.80	0.85	0.86	0.68	0.80	0.75	0.75
$12 + \log(O^{2+}/H^+)$	8.24±0.14	8.08±0.14	7.74±0.15	7.71±0.15	8.15±0.15	7.85±0.15	8.10±0.15	7.74±0.15
$12 + \log(O^+/H^+)$	8.39±0.09	8.38±0.14	8.30±0.15	8.29±0.15	8.47±0.15	8.35±0.15	8.28±0.15	8.40±0.15
$12 + \log(O/H)$	8.62±0.11	8.56±0.15	8.41±0.15	8.39±0.15	8.65±0.15	8.47±0.15	8.50±0.15	8.49±0.15
$12 + \log(S^+/H^+)$	6.29±0.06	6.40±0.08	6.07	6.10	6.49	6.31	6.37	6.31
$12 + \log(S^{2+}/H^+)$	6.75±0.05	6.58±0.10	6.56	6.50	6.83	6.52	6.61	6.66
$12 + \log(S/H)$	6.88±0.05	6.80±0.09	6.68	6.65	6.99	6.73	6.81	6.82
$\log(N/O)$	-1.03±0.06	-0.94±0.08	-1.01	-1.02	-0.87	-0.89	-0.79	-0.94
$\log(S/O)$	-1.74±0.14	-1.76±0.20	-1.73	-1.74	-1.66	-1.74	-1.69	-1.67

**Figure 7.** Wolf-Rayet feature at $\lambda 4686$ in region 74C.

for region 74C using different sets of models: those of Schaerer & Vacca (1998) for WR populations, and those of García-Vargas et al. (1995) and Leitherer et al. (1999) for ionizing populations, to try to reproduce simultaneously both the WR features and the emission-line spectrum. No consistent solution has been found. The models that better reproduce the WR features (a cluster 4.5 Myr old in the models of Schaerer & Vacca and Leitherer et al.) are too hard to reproduce the emission-line spectrum. Conversely, a cluster 5.3 Myr old in the model of García-Vargas et al. adequately reproduces the emission-line spectrum, but produces too few WR stars to explain the observed WR features.

When comparing the WR ‘bump’ and He II intensities and equivalent widths with other well-studied H II regions of different metallicities, the data on region 74C are found to fall into the observed ranges. However, the expected decrease of WR feature intensities with decreasing metallicity is not clearly observed. On the other hand, a decrease in the effective temperature of the ionizing radiation with increasing metallicity is apparent. This seems to imply that, while the number ratio of WR to O stars is similar for regions of metallicities differing by a factor of 3, the WR stars are cooler for the regions with higher metallicity.

Table 5. Single-star photoionization models for the observed H II regions.

Parameter	Region									
	74C		69C		5N		GA1		GA2	
	Model	Observed	Model	Observed	Model	Observed	Model	Observed	Model	Observed
$\langle \log U \rangle$	-2.55	-2.45 \pm 0.05	-2.70	-2.70 \pm 0.20	-2.90	-2.90 \pm 0.10	-2.85	-2.90 \pm 0.20	-2.85	-3.0 \pm 0.2
n_e (cm $^{-3}$)	50	60	10	<40	10	<40	10	<40	150	160
T_{eff} (K)	35 300	...	35 500	...	35 300	...	36 000	...	35 300	...
$12 + \log(\text{O}/\text{H})$	8.68	8.62 \pm 0.11	8.65	8.56 \pm 0.15	8.55	8.40 \pm 0.15	8.80	8.65 \pm 0.15	8.70	8.50 \pm 0.15
$12 + \log(\text{S}/\text{H})$	6.98	6.88 \pm 0.05	6.94	6.80 \pm 0.09	6.83	...	7.08	...	6.98	...
$\log(\text{N}/\text{O})$	-0.98	-1.03 \pm 0.06	-0.93	-0.94 \pm 0.08	-1.05	...	-1.00	...	-1.05	...
$\log(\text{S}/\text{O})$	-1.70	-1.74 \pm 0.14	-1.71	-1.76 \pm 0.20	-1.72	...	-1.72	...	-1.72	...
3727 [O II]	2.14	2.10 \pm 0.04	2.36	2.28 \pm 0.09	3.34	3.35 \pm 0.20	2.36	2.34 \pm 0.08	3.12	3.01 \pm 0.09
5007 [O III]	1.15	1.14 \pm 0.01	0.99	0.93 \pm 0.03	0.89	0.84 \pm 0.04	0.74	0.79 \pm 0.02	0.93	0.86 \pm 0.02
6584 [N II]	0.61	0.61 \pm 0.02	0.77	0.78 \pm 0.02	0.76	0.64 \pm 0.03	0.78	0.78 \pm 0.02	0.83	0.79 \pm 0.01
6716 [S II]	0.20	0.26 \pm 0.01	0.25	0.36 \pm 0.01	0.32	0.33 \pm 0.02	0.34	0.56 \pm 0.01	0.33	0.50 \pm 0.01
9069 [S III]	0.29	0.266 \pm 0.004	0.27	0.19 \pm 0.01	0.26	0.21 \pm 0.02	0.28	0.30 \pm 0.02	0.33	0.18 \pm 0.01
6312 [S III]	0.0075	0.009 \pm 0.001	0.0072	0.007 \pm 0.002
$\tau(\text{O}^{2+})$	0.66	0.69 \pm 0.04	0.68	0.72 \pm 0.05
$\tau(\text{O}^+)$	0.76	0.79 \pm 0.03	0.77	0.80 \pm 0.04

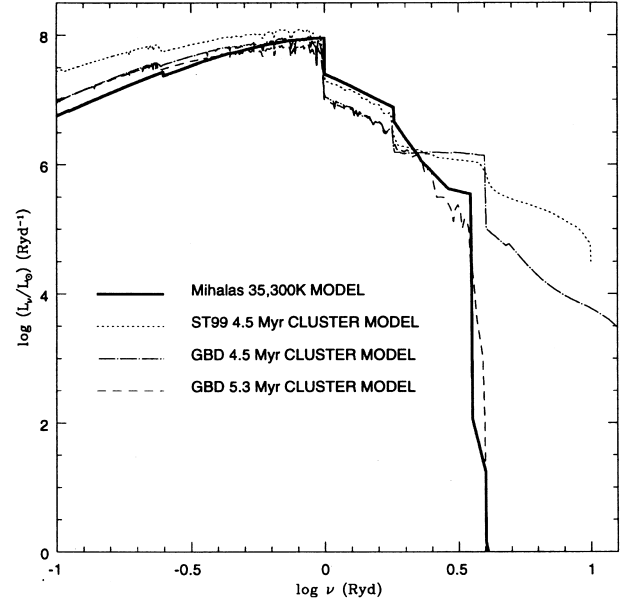


Figure 8. Spectral energy distribution of different ionizing clusters for region 74C.

Table 6. Physical properties of the observed H II regions.

Region	$L(\text{H}\alpha)$ ($10^{38} \text{ erg s}^{-1}$)	$Q(\text{H})$ (10^{49} s^{-1})	ϵ	$M(\text{H II})$ (M_{\odot})	M^{\star} (M_{\odot})
74C	32.1	148	0.10	78 200	112 000
69C	1.85	8.49	0.45	27 000	4 840
5N(A)	1.09	5.01	0.41	15 900	5 570
5N(B)	0.81	3.70	0.34	11 800	4 570
GA1	1.27	5.84	0.27	18 500	6 180
GA2	2.27	10.4	0.04	2 080	25 200
GA3	0.54	2.46	0.29	7 830	8 450
GA4	0.35	1.59	0.52	5 050	4 010

Table 7. Evolutionary models for region 74C.

Parameter	Observations	5.3 Myr model (GBD) ^a	4.5 Myr model (ST99) ^b
3727 [O II]	2100 \pm 40	2396	2181
5007 [O III]	1140 \pm 10	1366	2394
4959 [O III]	378 \pm 5	473	829
6548 [N II]	200 \pm 10	200	242
6584 [N II]	610 \pm 20	600	713
6717 [S II]	260 \pm 10	217	386
6731 [S II]	188 \pm 3	160	282
6312 [S III]	9 \pm 1	9	8
9069 [S III]	266 \pm 4	333	308
9532 [S III]	660 \pm 20	827	765
EW(H β) (Å)	81	100	97
$\log Q(\text{H})$	51.17	51.17	51.17
$\langle \log U \rangle$	-2.45 \pm 0.05	-2.30	-2.48
$\tau(\text{O}^+)$	0.79 \pm 0.03	0.76	0.81
$\tau(\text{O}^{2+})$	0.69 \pm 0.04	0.66	0.69
Z/Z_{\odot}	0.5	0.65	0.65

^a García-Vargas, Bressan & Díaz (1995).

^b Leitherer et al. (1999; STARBURST99).

Table 8. WR feature intensities and equivalent widths in region 74C and other extragalactic H II regions.

Region	$L(\text{WR})/\text{H}\beta$	$\text{EW}(\text{WR})$ (Å)	$L(\text{He II})/\text{H}\beta$	$\text{EW}(\text{He II})$ (Å)	$12 + \log(\text{O}/\text{H})$	T_{eff} (K)
Region A (NGC 3310)	0.16	5.7	0.11	3.9	8.21	40 000
NGC 604 (M33)	0.12	10.3	0.06	5.2	8.40	37 000
Region A (NGC 7714)	0.07	1.5	0.05	1.0	8.47	36 000
Region 74C (NGC 4258)	0.15	10.8	0.09	6.6	8.62	35 300

Both more observations of confirmed high-metallicity regions and a finer metallicity grid for the evolutionary synthesis models are needed in order to understand the ionizing populations of H II regions.

ACKNOWLEDGMENTS

The WHT is operated on the island of La Palma by the Isaac Newton Group in the Spanish Observatorio del Roque de los Muchachos of the Instituto de Astrofísica de Canarias. We would like to thank CAT for awarding observing time.

ET is grateful to an IBERDROLA Visiting Professorship to UAM during which part of this work was completed. This work has been partially supported by DGICYT project PB-96-052.

We also thank an anonymous referee for helpful suggestions.

REFERENCES

- Bressan A., Fagotto F., Bertelli G., Chiosi C., 1993, *A&AS*, 100, 647
 Brocklehurst M., 1971, *MNRAS*, 153, 471
 Cecil G., Morse J. A., Veilleux S., 1995, *ApJ*, 452, 613
 Cerviño M., Mas-Hesse J. M., 1994, *A&A*, 284, 749
 Courtés G., Cruvellier P., 1961, *A&A*, 200, 58
 Courtés G., Petit H., Hua C. T., Martin P., Blecha A., Huguenin D., Golay M., 1993, *A&A*, 268, 419(C93)
 Deharveng J. M., Pellet A., 1970, *A&A*, 9, 181
 de Vaucouleurs G., de Vaucouleurs A., Corwin H. G., 1976, *Second Reference Catalogue of Bright Galaxies*
 Díaz A. I., Tenorio-Tagle G., 1994, in Tenorio-Tagle G., ed., *Violent Star Formation: From 30 Doradus to Quasars*. Cambridge Univ. Press, Cambridge, p. 105
 Díaz A. I., 1999, *Ap&SS*, 263, 143
 Díaz A. I., Pérez-Montero E., 2000, *MNRAS*, 312, 130
 Díaz A. I., Pagel B. E. J., Wilson I. R. G., 1985, *MNRAS*, 212, 737
 Díaz A. I., Terlevich E., Pagel B. E. J., Vílchez J. M., Edmunds M. G., 1987, *MNRAS*, 226, 19
 Díaz A. I., Terlevich E., Vílchez J. M., Pagel B. E. J., Edmunds M. G., 1991, *MNRAS*, 253, 245
 Fagotto F., Bressan A., Bertelli G., Chiosi C., 1994, *A&AS*, 105, 39
 Ferland G. J., 1996, *HAZY: A Brief Introduction to CLOUDY*. Internal report, Univ. Kentucky,
 García-Vargas M. L., Díaz A. I., 1994, *ApJS*, 91, 553
 García-Vargas M. L., Bressan A., Díaz A. I., 1995, *A&AS*, 112, 35
 García-Vargas M. L., González-Delgado R. M., Pérez E., Alloin D., Díaz A. I., Terlevich E., 1997, *ApJ*, 478, 112
 Garnett D. R., 1992, *AJ*, 103, 1330
 González-Delgado R. M., Pérez E., 1996, *MNRAS*, 281, 781
 González-Delgado R. M. et al., 1994, *ApJ*, 437, 239
 González-Delgado R. M., Pérez E., Tadhunter C., Vílchez J. M., Rodríguez-Espinosa J. M., 1997, *ApJS*, 108, 155
 González-Delgado R., Heckman T. M., Leitherer C., Meurer G. R., Krolík J., Wilson A. S., Kinney A., Koratkar A., 1998, *ApJ*, 505, 174
 Heckman T. M., 1980, *A&A*, 87, 142
 Heckman T. M., González-Delgado R., Leitherer C., Meurer G. R., Krolík J., Wilson A. S., Koratkar A., Kinney A., 1997, *ApJ*, 482, 114
 Hummel E., Krause M., Lesch H., 1989, *A&A*, 211, 266
 Kennicutt R. C., 1983, *ApJ*, 272, 54
 Kunth D., Sargent W. L. W., 1983, *ApJ*, 273, 81
 Leitherer C. et al., 1999, *ApJS*, 123, 3
 McGaugh S. S., 1991, *ApJ*, 380, 140
 Martin P., Roy J. R., Noreau L., Lo K. Y., 1989, *ApJ*, 345, 707
 Meynet G., Maeder A., Schaller G., Schaerer D., Charbonnel C., 1994, *A&AS*, 103, 97
 Miyoshi M., Moran J., Herrnstein J., Greenhill L., Nakai N., Diamond P., Inoue M., 1995, *Nat*, 373, 127
 Oey M. S., Kennicutt R. C., 1993, *ApJ*, 411, 137
 Osterbrock D. E., 1989, *Astrophysics of Gaseous Nebulae and Active Galactic Nuclei*, University Science Books, Mill Valley
 Osterbrock D. E., Fulbright J. P., Bida T. A., 1997, *PASP*, 109, 614
 Pagel B. E. J., Simonson E. A., Terlevich R. J., Edmunds M. G., 1992, *MNRAS*, 255, 325
 Panagia N., 1973, *AJ*, 78, 929
 Pastoriza M. G., Dottori H. A., Terlevich E., Terlevich R., Díaz A. I., 1993, *MNRAS*, 260, 177
 Pérez E., 1997, *MNRAS*, 290, 465
 Phillips M. M., Pagel B. E. J., Edmunds M. G., Díaz A. I., 1984, *MNRAS*, 210, 701
 Roy J. R., Arsenault R., Joncas G., 1986, *ApJ*, 300, 624
 Sandage A., Tammann G., 1981, *A Revised Shapley-Ames Catalog of Bright Galaxies*. Carnegie Inst. Washington, Washington D.C., p. 42
 Schaerer D., Vacca W. D., 1998, *ApJ*, 497, 618
 Smith L. F., van der Hucht K. A., Hidayat B., 1991, *Proc. IAU Symp.* 143, Wolf-Rayet Stars and Interrelations with Other Massive Stars in Galaxies, Kluwer, Dordrecht, p. 601
 Smith L. F., Shara M. M., Moffat A. F. J., 1996, *MNRAS*, 281, 163
 Stasińska G., 1980, *A&A*, 84, 320
 Stasińska G., Leitherer C., 1996, *ApJS*, 107, 661
 Stauffer J. R., 1982, *ApJ*, 262, 66
 Stüwe J. A., Schulz H., Hühnermann H., 1992, *A&A*, 261, 382
 Tayal S. S., 1997, *ApJ*, 481, 550
 Terlevich E., Díaz A. I., Terlevich R., González-Delgado R. M., Pérez E., García-Vargas M. L., 1996, *MNRAS*, 279, 1219
 Terlevich R., Melnick J., 1985, *MNRAS*, 213, 841
 Terlevich R., Tenorio-Tagle G., Franco J., Melnick J., 1992, *MNRAS*, 255, 713
 Vacca W. D., Conti P. S., 1992, *ApJ*, 401, 533

This paper has been typeset from a \LaTeX file prepared by the author.